

The polarized sky: 1957-2017

M.A. Brentjens

Radio Observatory & R&D
ASTRON, Dwingeloo, The Netherlands

July 6, 2017

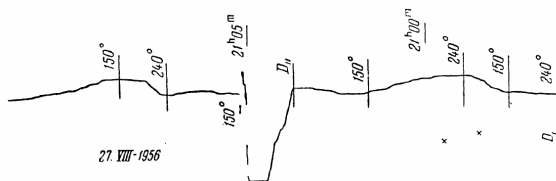


Fig. 1. Sample of the recordings obtained during the measurement of the linear polarization of the cosmic radio radiation at a wavelength of 1.45 m from a region in the sky with a high galactic latitude ($b = +25^\circ$). As can be seen from the figure, a rotation of the antenna plane through 90° , relative to the girder on which it is held, results in a change in sign of the difference $I_{150^\circ} - I_{240^\circ}$.

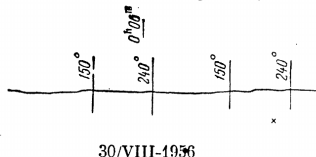


Fig. 2. Sample of the recordings obtained during the measurement of the polarization of the cosmic radio radiation at a wavelength of 1.45 m when the electrical axis of the antenna lies in the galactic plane.

The effect illustrated by Figs. 1 and 2 is confirmed by numerous measurements of the cosmic radio radiation at a wavelength of 1.45 m. The main result of these measurements is that the results of the earlier measurements stated as follows. When the electrical axis of the antenna forms an angle greater than 5° with the normal to the galactic plane, the rotation of the antenna about the normal results in a characteristic variation in the polarization received. On the other hand, when the electrical axis of the antenna lies in the galactic plane,

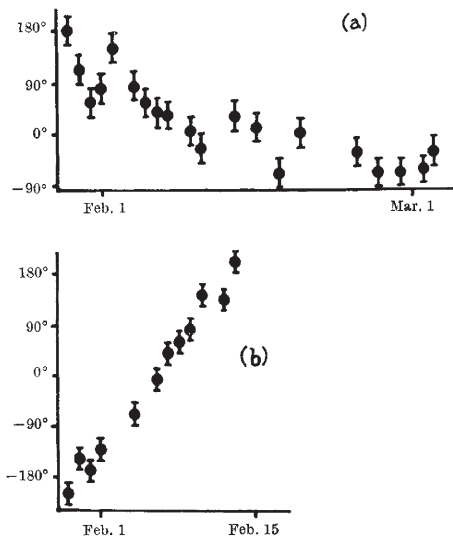


Fig. 1. Plots of the position angle against time of the planes of polarization for the areas centred on (a) R.A. 05h., declination 22° N.; (b) R.A. 18h., declination 22° N. The origin of the ordinate corresponds to polarization in the plane of the meridian

BULLETIN OF THE ASTRONOMICAL INSTITUTES
OF THE NETHERLANDS

1962 JULY 6

VOLUME XVI

NUMBER 518

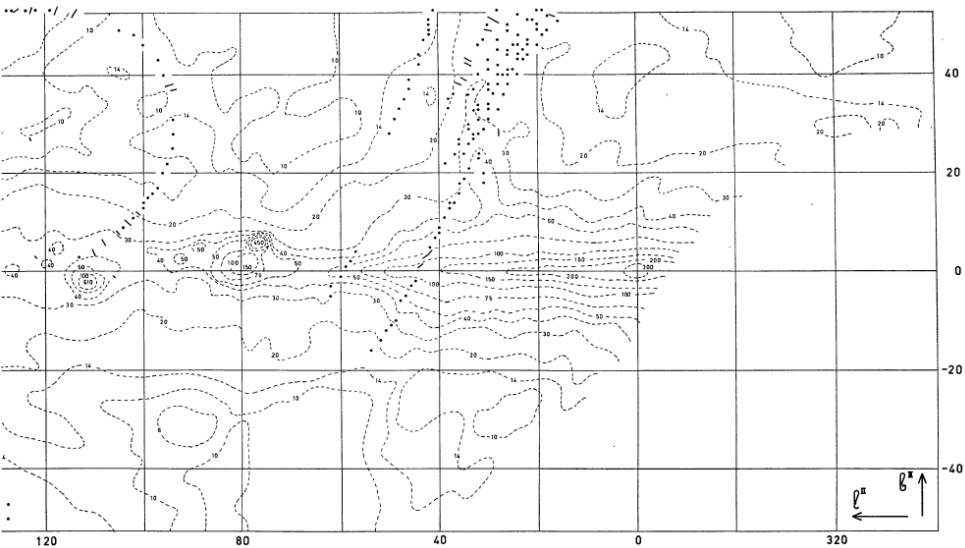
COMMUNICATIONS FROM THE OBSERVATORY AT LEIDEN AND
THE NETHERLANDS FOUNDATION FOR RADIO ASTRONOMY

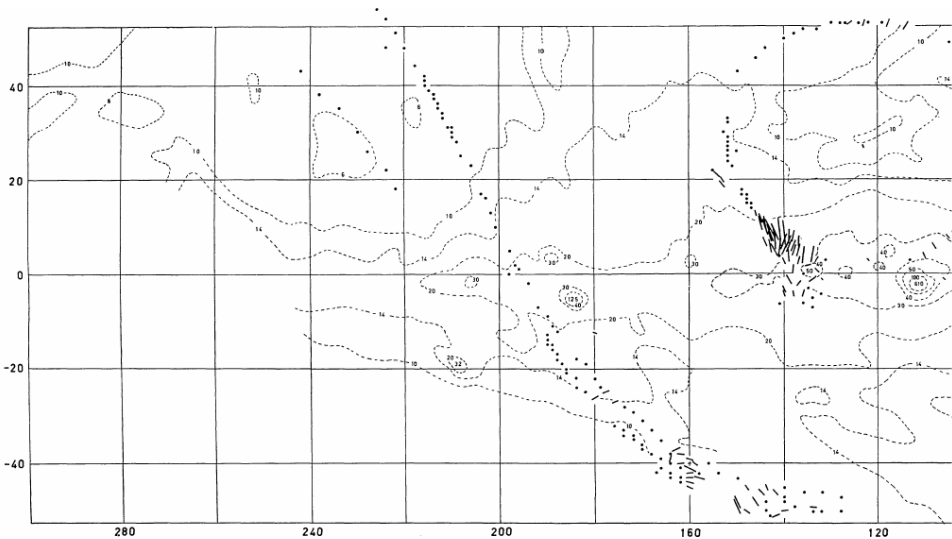
POLARIZATION OF THE GALACTIC 75-CM RADIATION

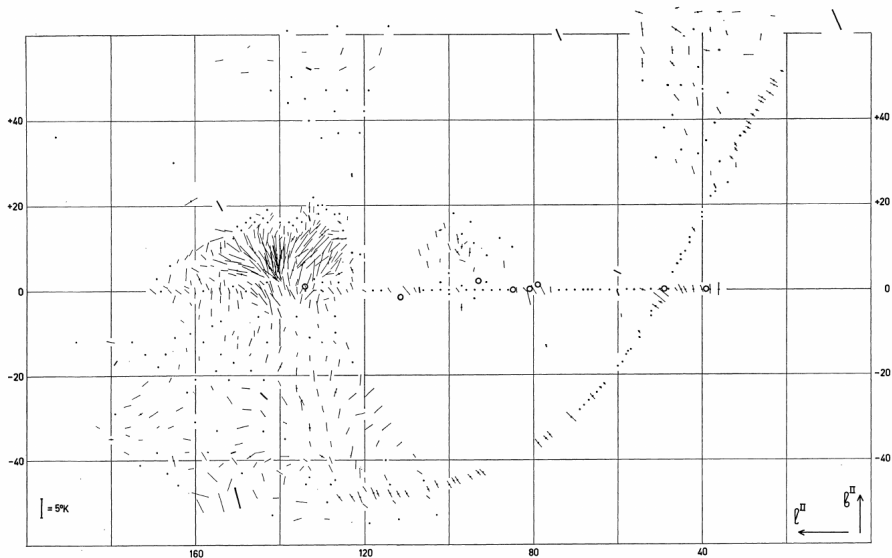
BY GART WESTERHOUT, CH. L. SEEGER,
W. N. BROUW AND J. TINBERGEN

CONTENTS

POLARIZATION OF THE GALACTIC 75-CM RADIATION	<i>Gart Westerhout, Ch. L. Seeger, W. N. Brouw and J. Tinbergen</i>	187
FURTHER POLARIZATION MEASUREMENTS AT 75 CM	<i>W. N. Brouw, C. A. Muller and J. Tinbergen</i>	213







Polarization measurements at 75 cm. The length and direction of the lines indicate \overline{T}_B^{Π} and θ_{pol} . Thick lines refer to measurements made five times or more,

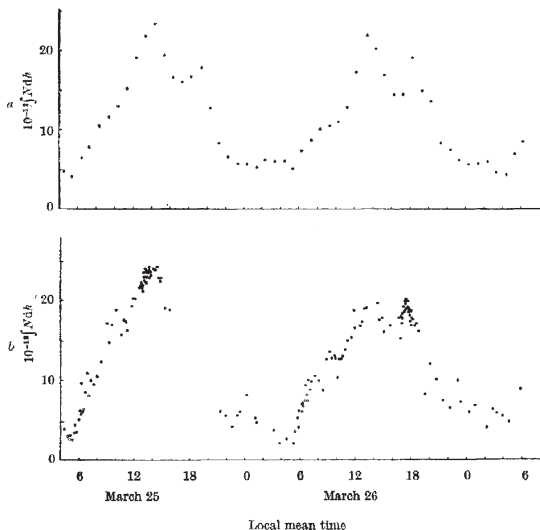


Fig. 2. *a*, Electron content of the ionosphere, derived from ionospheric soundings; *b*, total electron content of the ionosphere as a function of local mean time derived from the polarization measurements

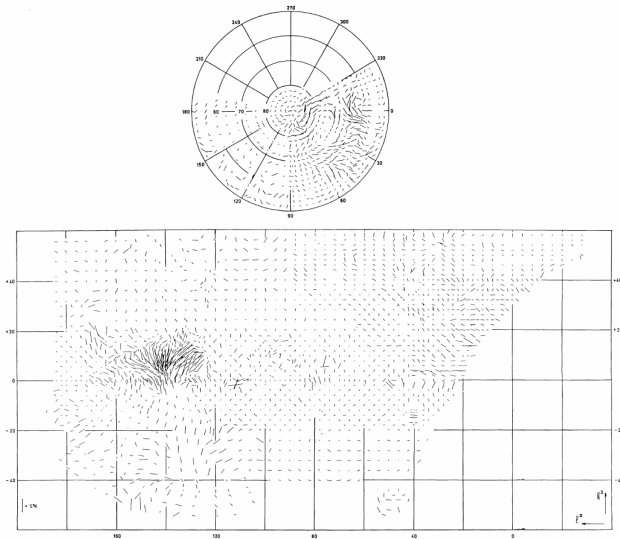


Figure 3. Polarization measurements at 75 cm. The length and the direction of the lines indicate \overline{T}_p and θ_{gal} . Only those results are plotted which were obtained from two or more independent measurements.

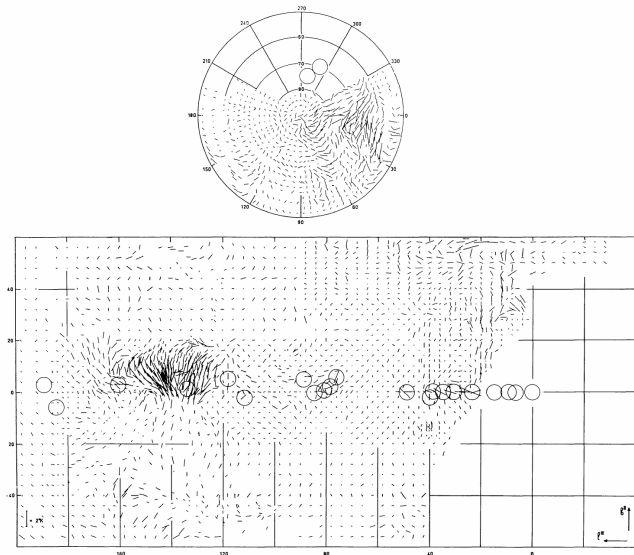


Figure 7. Polarization map at 610 Mc/s. The length and direction of the lines indicate $\overline{T_p^p}$ and θ_{gal} . Only those results were plotted which were obtained from two or more independent measurements. The circles show the positions of the strongest point sources. Only measurements within the circles could be affected by the sources.

As in reference (10) we superpose all the radiation from the same Faraday depth and write $E(\phi)$ for the fraction of the radiation with Faraday depth ϕ and $P(\phi)$ for its intrinsic polarization. Defining the 'Faraday dispersion function' as $F(\phi) = E(\phi)P(\phi)$, we obtain the Fourier transform relation

$$P(\lambda^2) = \int_{-\infty}^{\infty} F(\phi) e^{2i\phi\lambda^2} d\phi. \quad (11)$$

It would be very convenient to be able to invert this transform and so obtain the Faraday dispersion function from the relation

$$F(\phi) = \pi^{-1} \int_{-\infty}^{\infty} P(\lambda^2) e^{-2i\phi\lambda^2} d(\lambda^2). \quad (12)$$

However, to evaluate this integral we must know $P(\lambda^2)$ for $\lambda^2 < 0$, and this is not an observable quantity. It is readily seen from equation (11) that this is the polarization we would observe if all of the Faraday rotation were in the opposite sense (i.e. if all the magnetic fields were reversed).

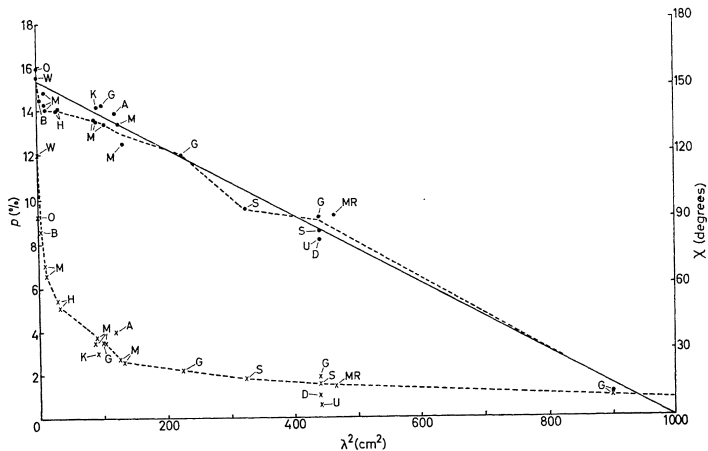


FIG. 3. Summary of the polarization data. The dots (·) and crosses (×) represent the observed angles and degrees of polarization. The solid line is the best fitting straight line through the dots for $\lambda > 9$. The broken lines show the assumed dependence of polarization on wavelength for the calculation of the Faraday dispersion function. O, Oort & Walraven (12); W, Woltjer (14); B, Boland et al. (21); M, Mayer et al. (9); H, Hollinger et al. (22); K, Kuzmin & Udaltsov (23); A, Altenhoff et al. (24); G, Gardner & Whiteoak (7); S, Seielstad et al. (25); D, Davies & Verschuur (26); U, Udaltsov (27); MR, Morris & Radhakrishnan (28).

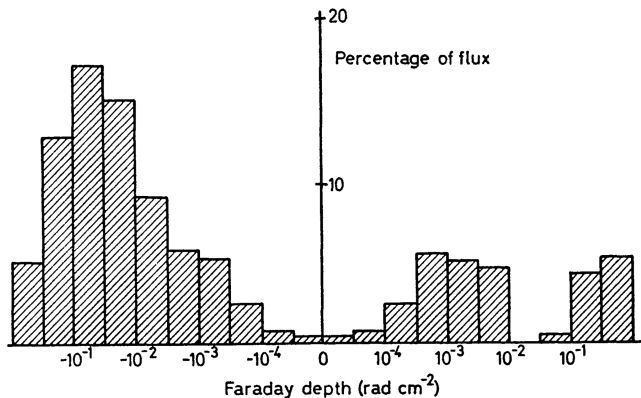
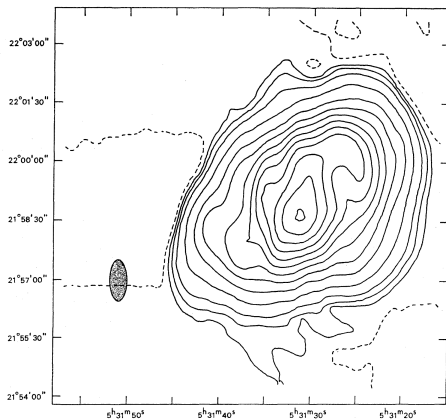
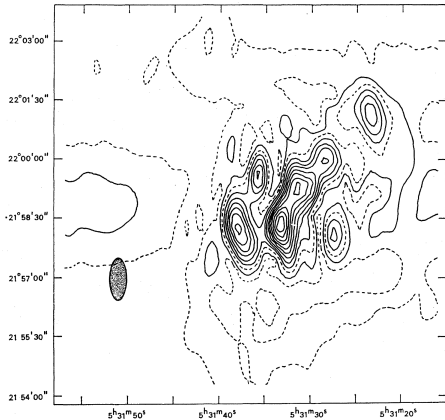


FIG. 4. *Faraday dispersion function of the Crab nebula. The rotation measure is taken as the zero of Faraday depth.*

Stokes I



P



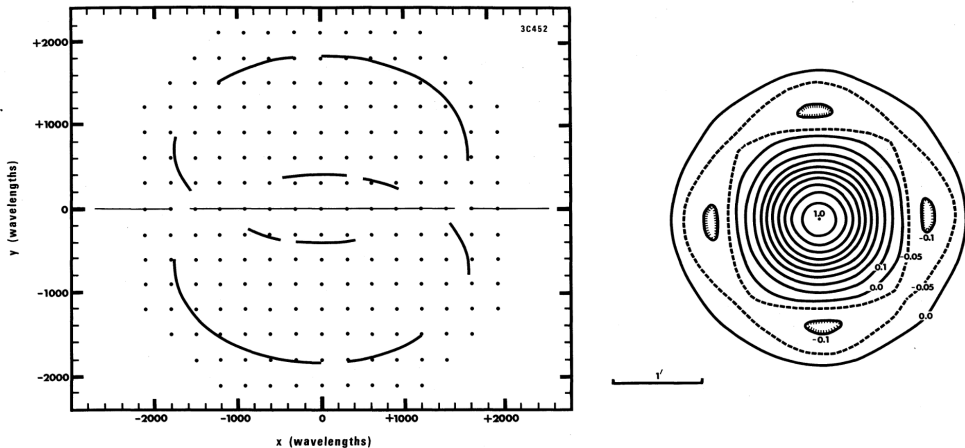
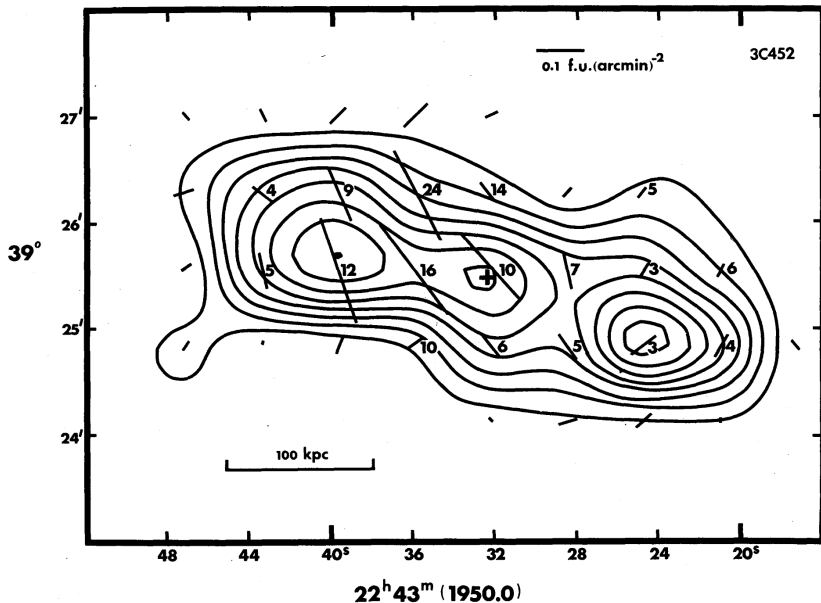


FIG. 1.—(a) (left) The portion of the Fourier transform plane sampled by the present observations (*heavy curves*) and by those of Fomalont (1967a) and Seielstad and Weiler (1969) (*light horizontal lines*). (b) (right) The equivalent scanning beam, assuming correctly interpolated values at the grid points. Interpolation errors will in practice produce errors in the derived distributions which correspond to distortions in the beam shown.



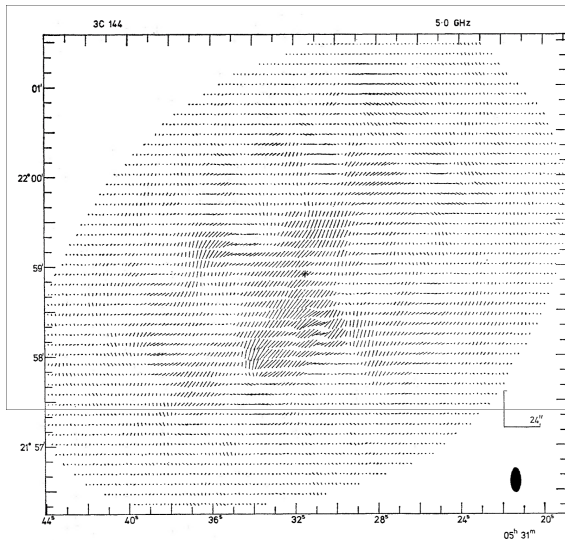
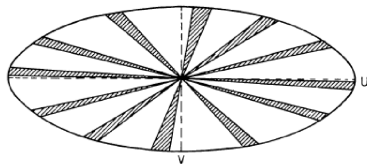
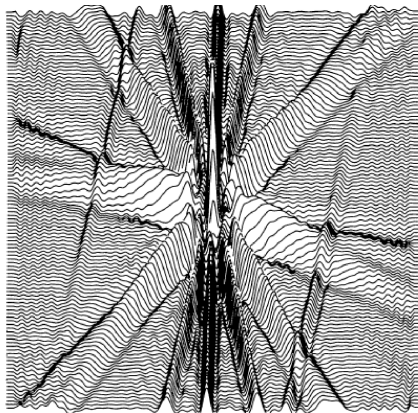
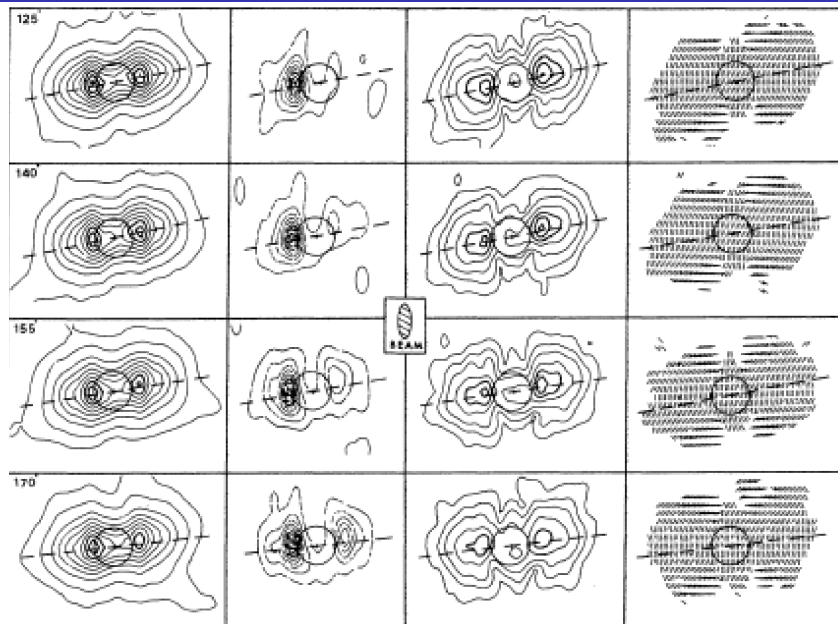


FIG. 7. The polarization vectors at 5.0 GHz. The direction of each line is that of the E vector and its length is proportional to the polarized flux density. The flux scale is such that the vector at the position of the pulsar (the cross) is 12.8 per cent of the total intensity. Its position angle is 135° . The beam is shown in the bottom right-hand corner. The vectors are drawn at intervals of 2.5 arc in right ascension and 6.677 arc in declination.



— = 4.8

Fig. 1a and b. Part **a** shows schematically the filling of the Fourier transform plane used to map Jupiter according to the method described in the text. The coordinates U (east-west) and V (north-south) refer to the length of a baseline projected onto the sky. Part **b** shows a typical beam pattern for our observations



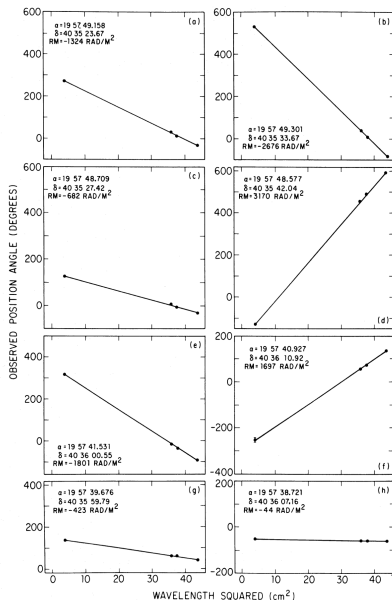


FIG. 2.—Examples of the fits of γ vs. λ^2 at eight locations in Cygnus A. Each point is plotted with its error bar—in most cases, the errors are smaller than the plotted dots. The coordinates and best fitting slope are printed inside each box.

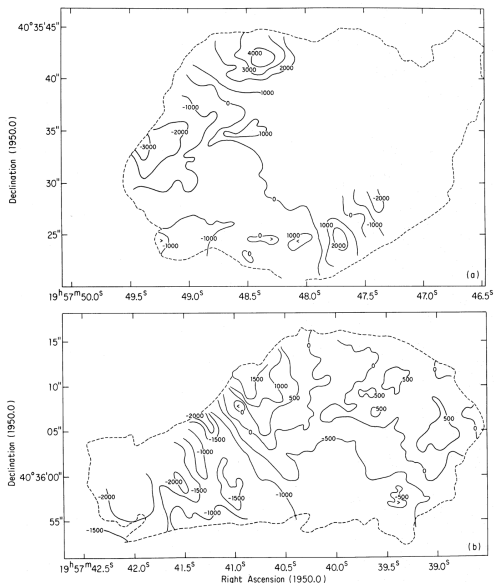


FIG. 3.—The distribution of rotation measure for Cygnus A, derived as explained in the text. The dashed line gives the boundaries of the radio lobes. Contour lines that end within the lobes indicate regions in which insufficient polarized brightness exists to determine the rotation measure. In particular, note that no fits were possible throughout nearly half the eastern lobe. The situation in the western lobe is much better.

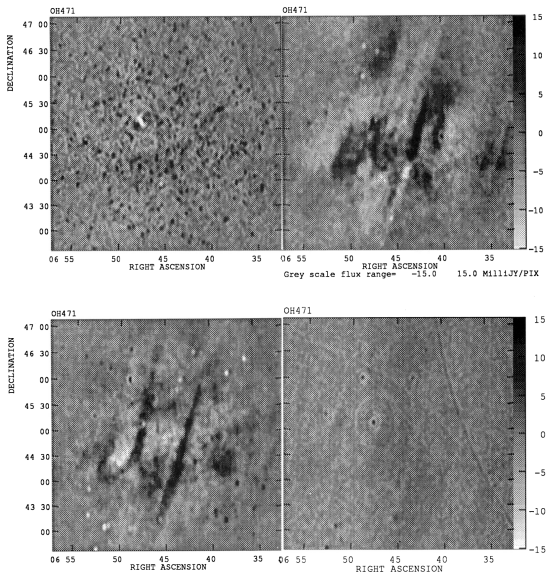


Fig. 1. Maps of Stokes I, Q (upper right), U and V polarization for the OH471 field, at 4' resolution; note the strong filament in PA. $\sim 160^\circ$, with indications of at least two more 'parallel' filaments; note also the clumpy structure; from the 1 map all sources with a flux density exceeding 5 mJy have been subtracted; the grey scale ranges from -15 to 15 mJy/beam

**NETHERLANDS FOUNDATION FOR
RESEARCH IN ASTRONOMY**

NOTE 655

RM-synthesis via wide-band low-frequency polarimetry

MAART 1996

BY A.G. de Bruyn

Future applications

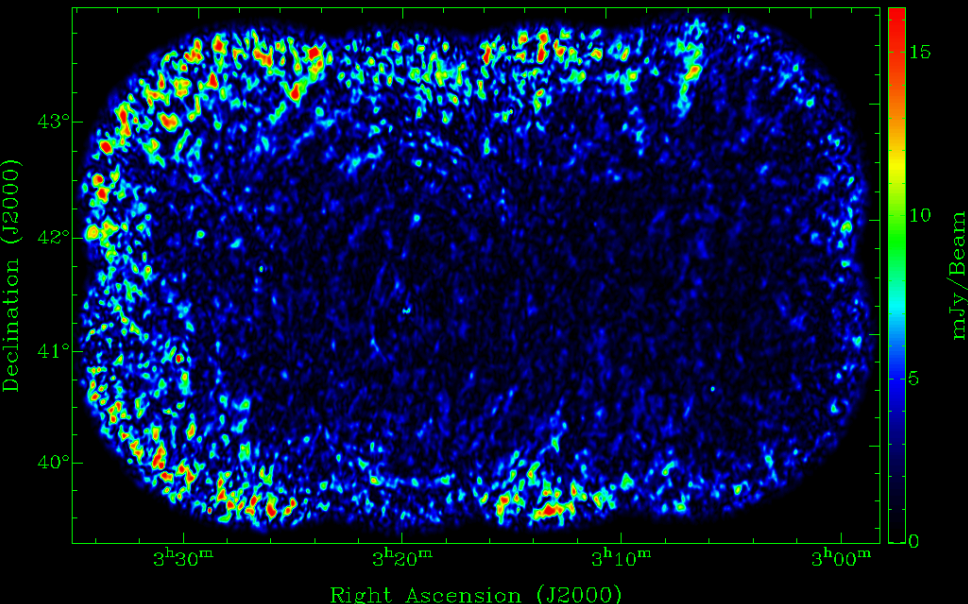
We expect the new tool to be particularly powerful in the study of weakly polarized extended sources, such as giant radio galaxies where the RM 's are known to be small. Small changes in the RM across the surface of extended sources should be easily traceable, especially if these RM s are showing some spatial coherence.

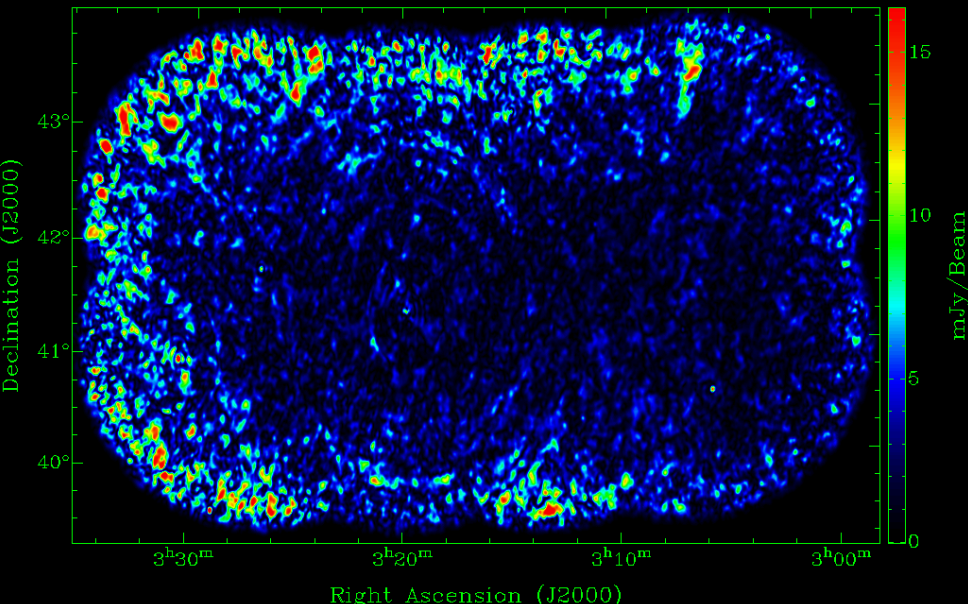
The wideband spectrometer (the DZB) currently being built for the WSRT makes it possible to search for and study weakly polarized structure over a much wider range of RM . The side-lobe levels in the RMTF that occur with an 8-channel system will be much reduced when 128 frequency channels can be used to cover a wide (80 MHz) low frequency band.

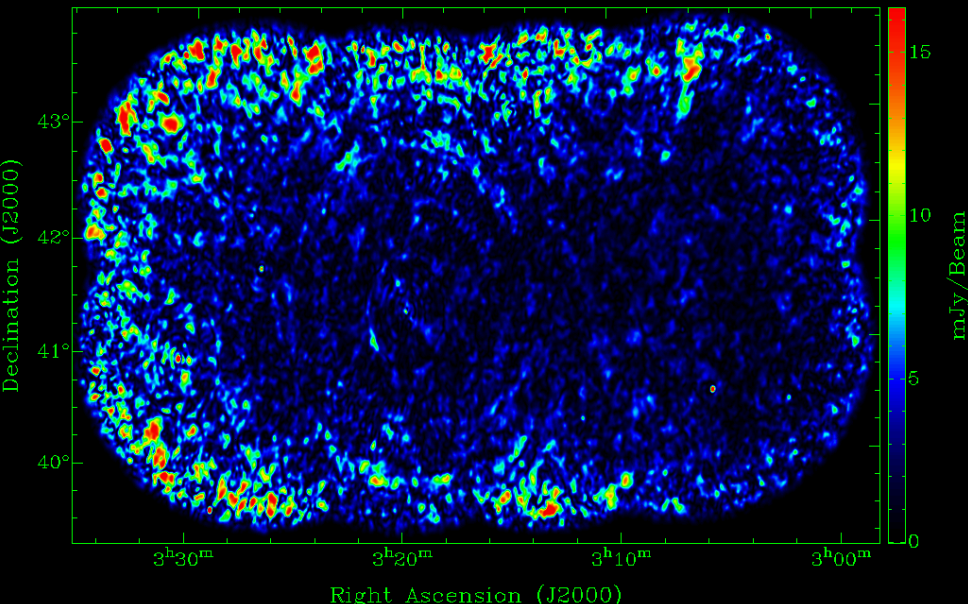
Very small variations in RM can be expected to occur close to the core of AGN when polarized structure moves relative to a foreground Faraday screen. With a sensitivity of 0.1 rad/m^2 extremely sensitive measurements of the ionized gas around polarized radio sources can be made. If several sources with a well-determined RM are found within the synthesized field of view the fundamental limit imposed by the uncertainty of the ionospheric RM can be avoided by the study of *differential* RM variations. The diffuse galactic background emission, which is highly polarized at low frequencies, and has a typical RM of $\approx 5\text{-}10 \text{ rad/m}^2$, may well be useful as a non-variable RM reference.

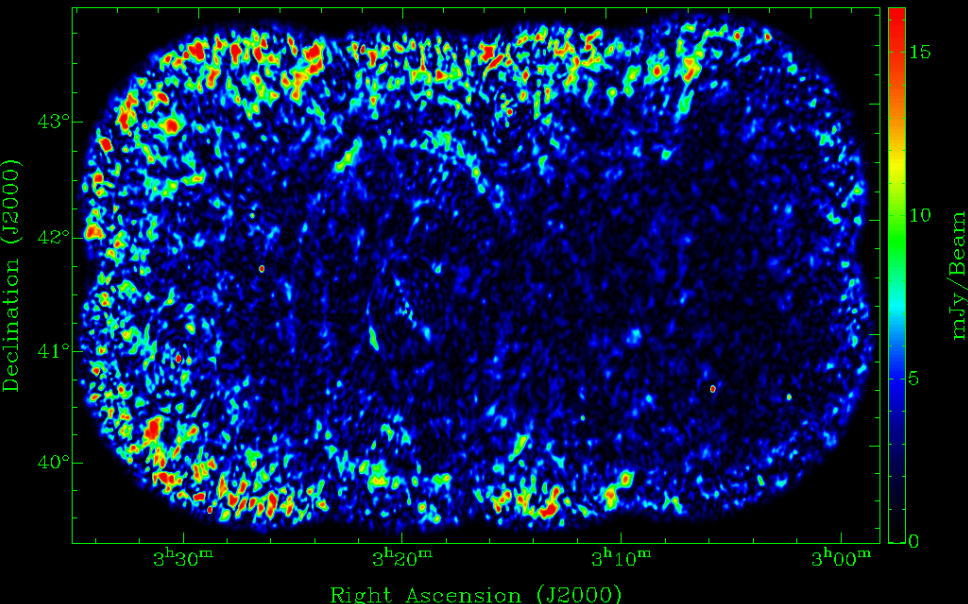
The range in RM where the RM-synthesis technique will be a useful tool depends on frequency. At 1400 MHz, and a bandwidth of 160 MHz, this range begins at a few hundred rad/m^2 . A practical limit, in real radio sources, will occur when depolarization due to fine-scale structure in RM within the beam, i.e. beam-depolarization, begins to dominate over bandwidth-depolarization.

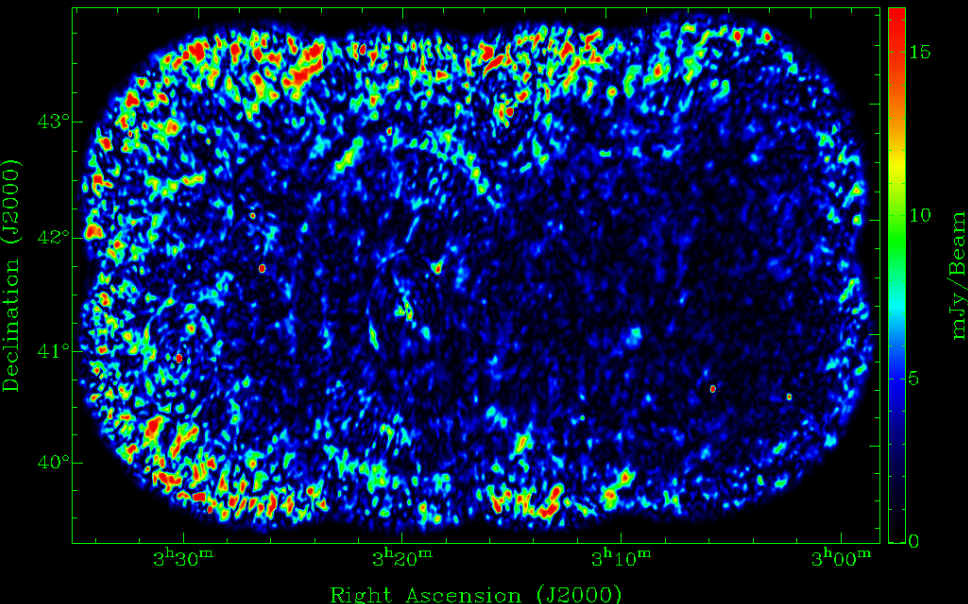
A final intriguing possibility opened up by low frequency wide-band polarimetry is the study of the Faraday rotating material *within* radio sources. The Fourier-relationship between the complex polarization and the 'Faraday depth' suggests that observations over a large range in frequency may be used to derive information about the spatial disposition of the emitting and depolarizing material.

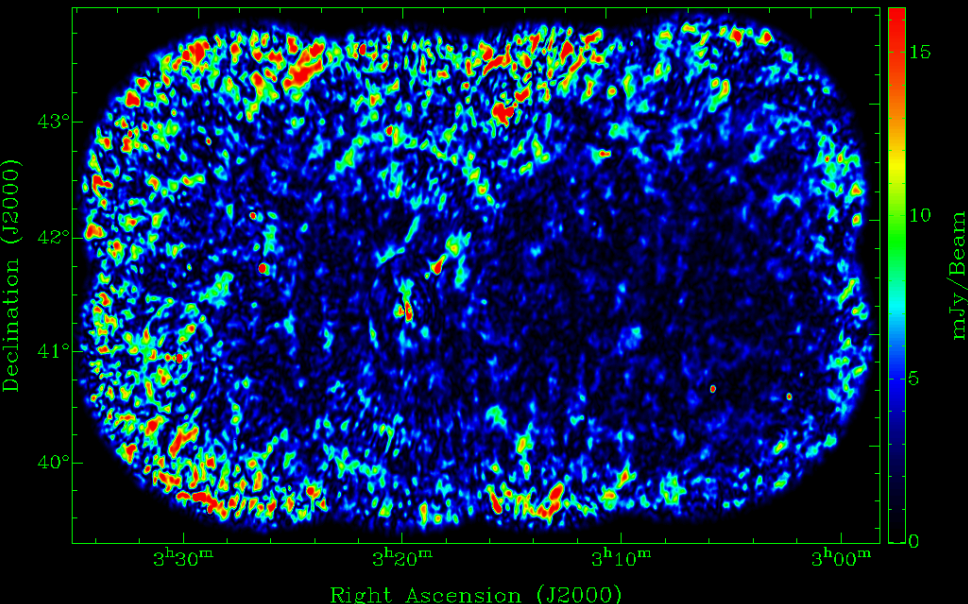
STOKES: $-2.400000e+01$ 

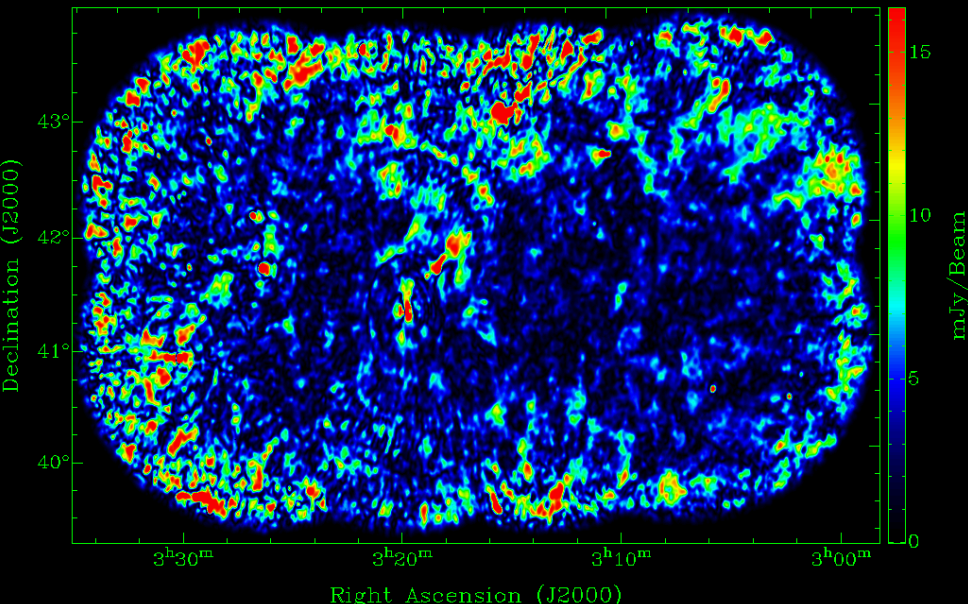
STOKES: $-2.100000e+01$ 

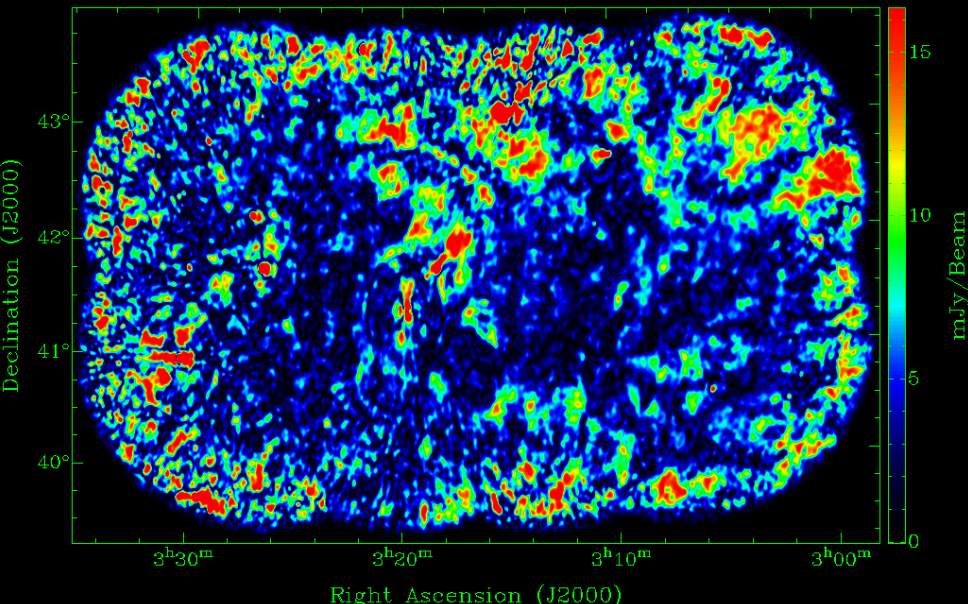
STOKES: $-1.800000e+01$ 

STOKES: $-1.500000e+01$ 

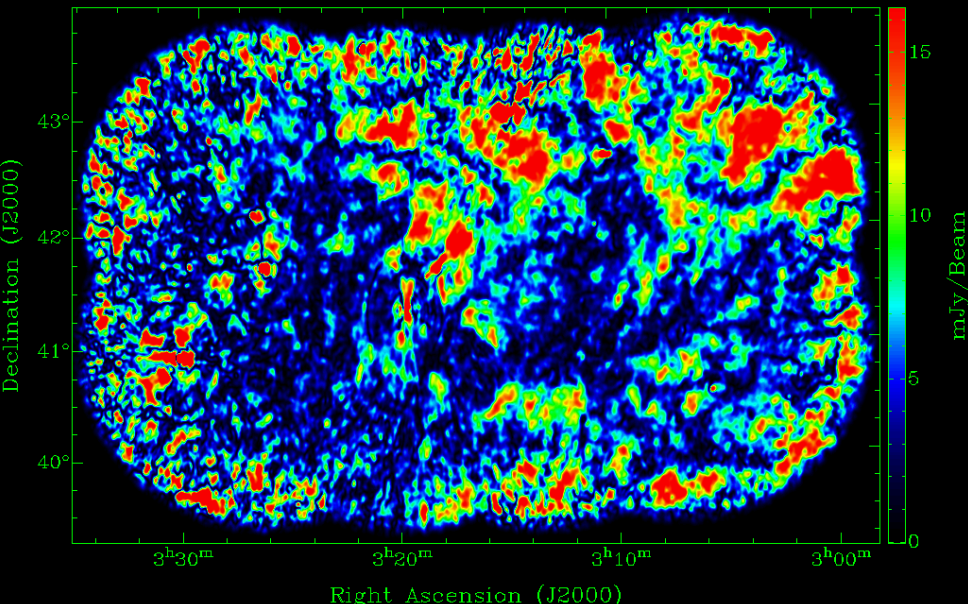
STOKES: $-1.200000e+01$ 

STOKES: $-9.000000e+00$ 

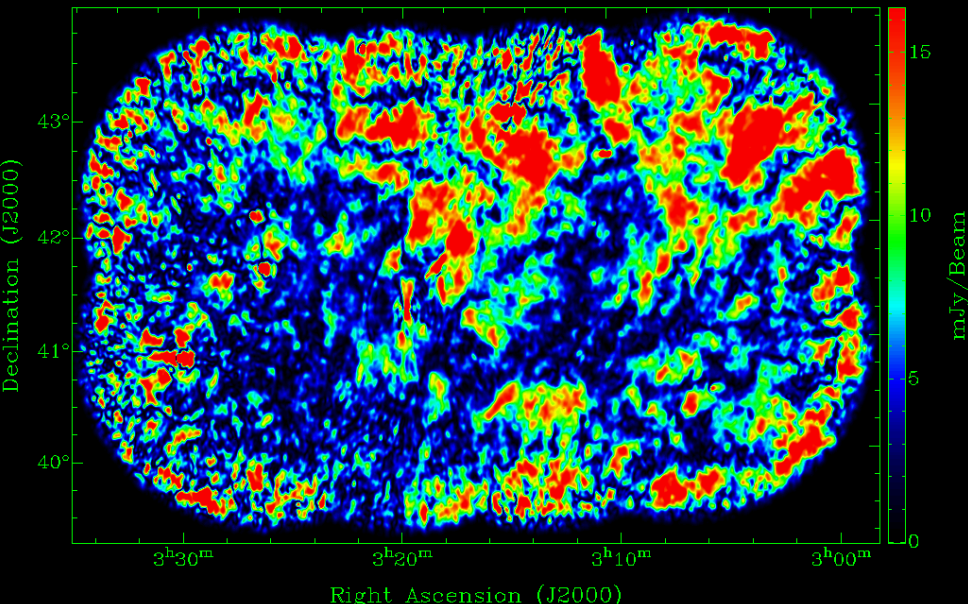
STOKES: $-6.000000e+00$ 

STOKES: $-3.000000e+00$ 

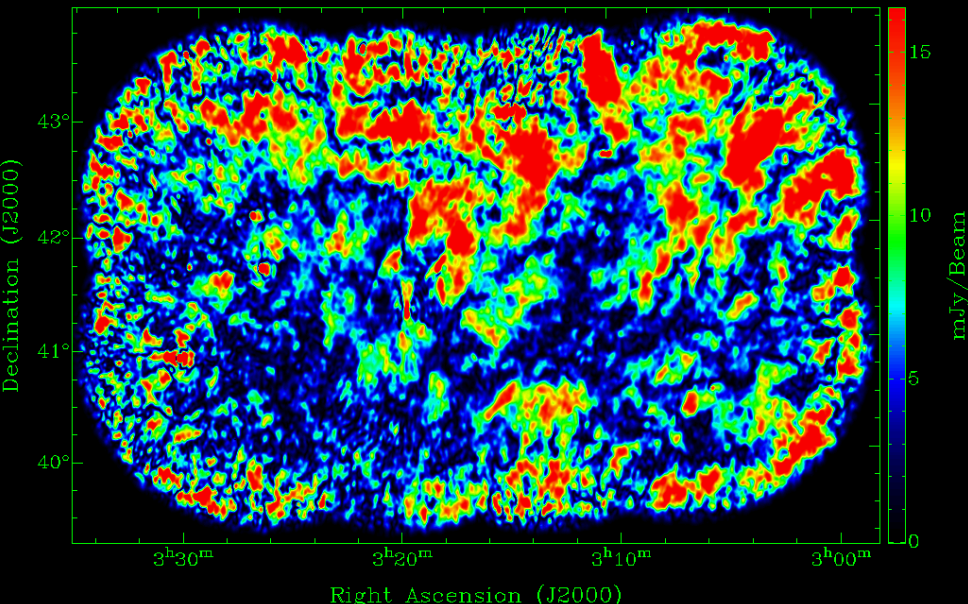
STOKES: 0.000000e+00



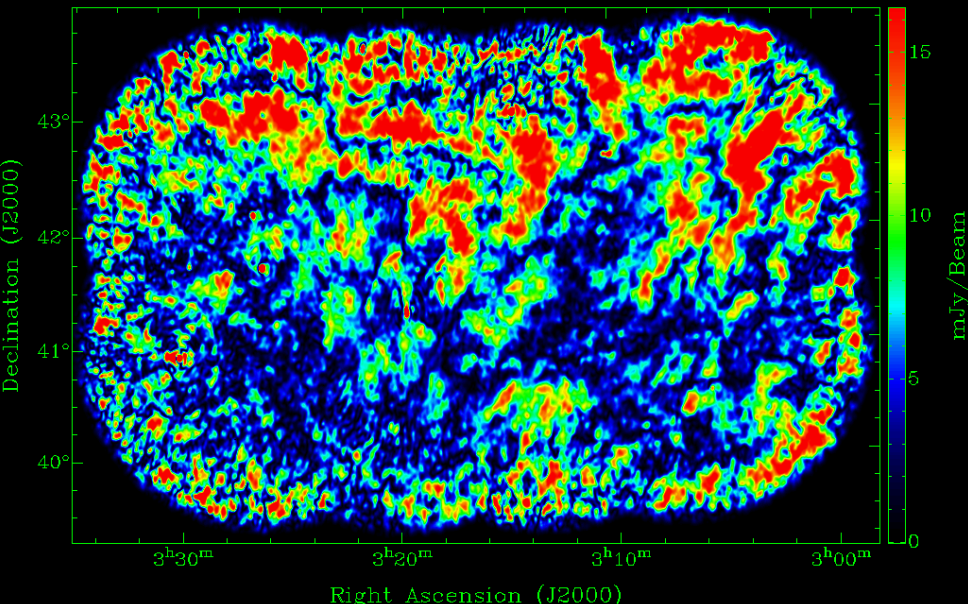
STOKES: 3.000000e+00



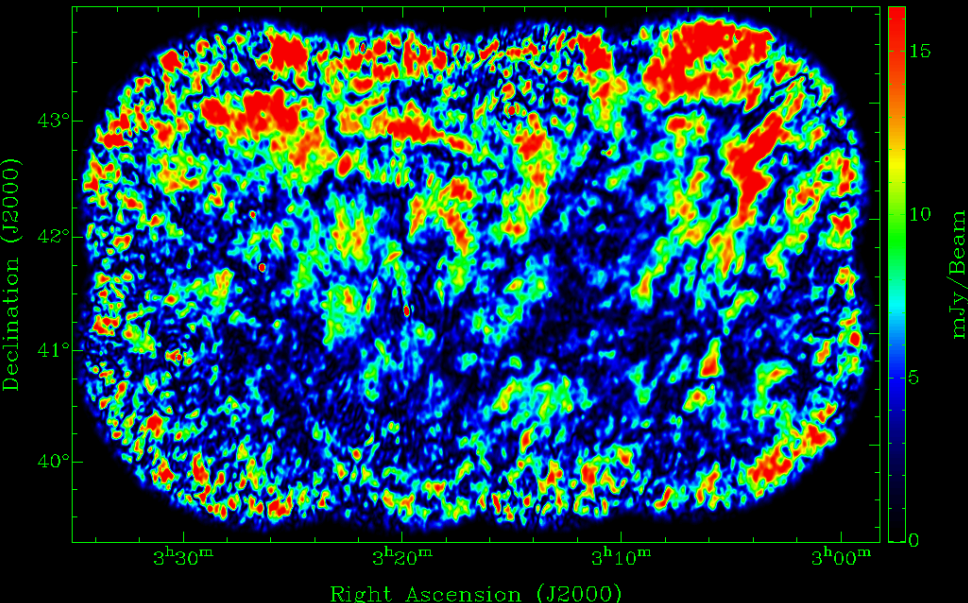
STOKES: 6.000000e+00



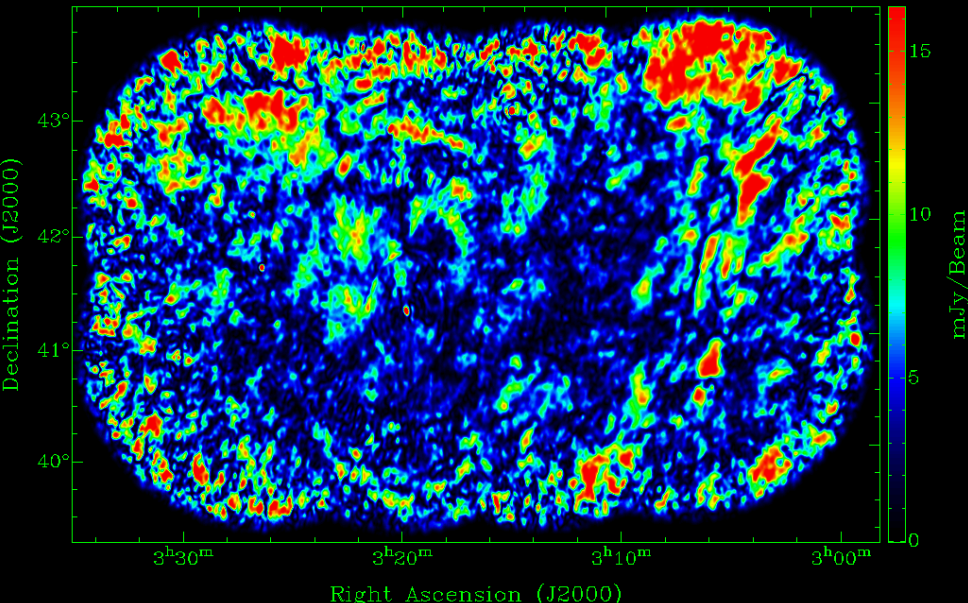
STOKES: 9.000000e+00



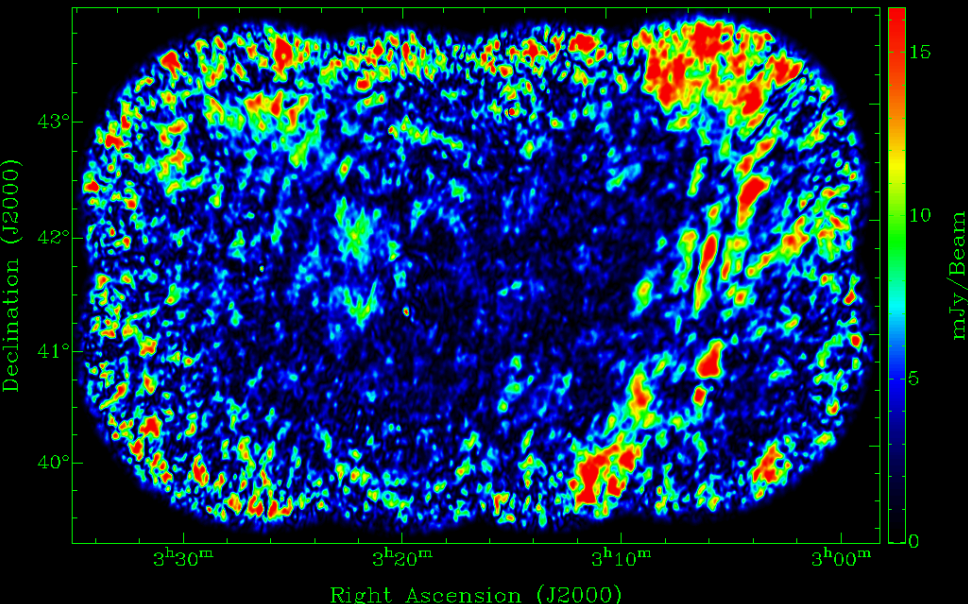
STOKES: 1.200000e+01



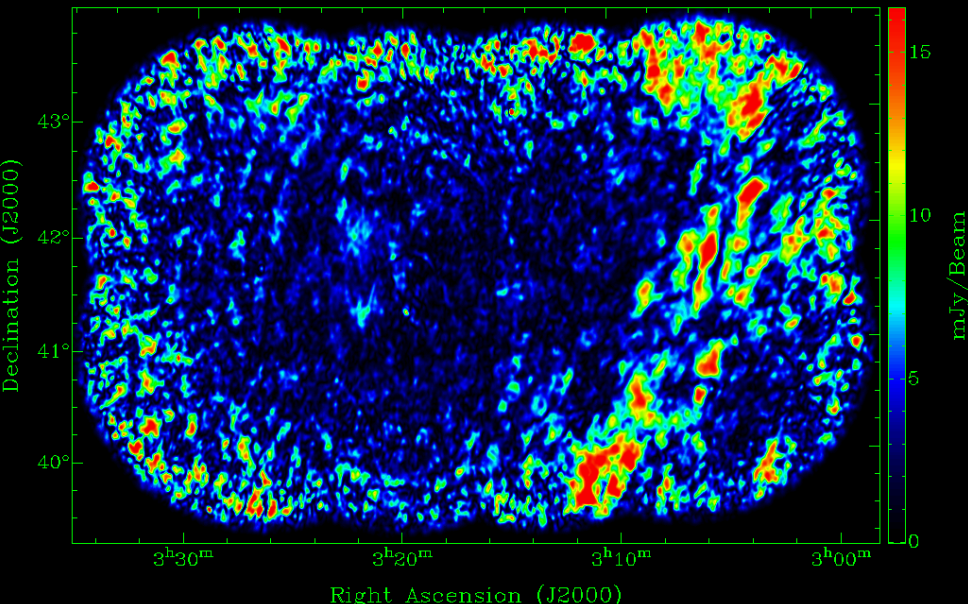
STOKES: 1.500000e+01



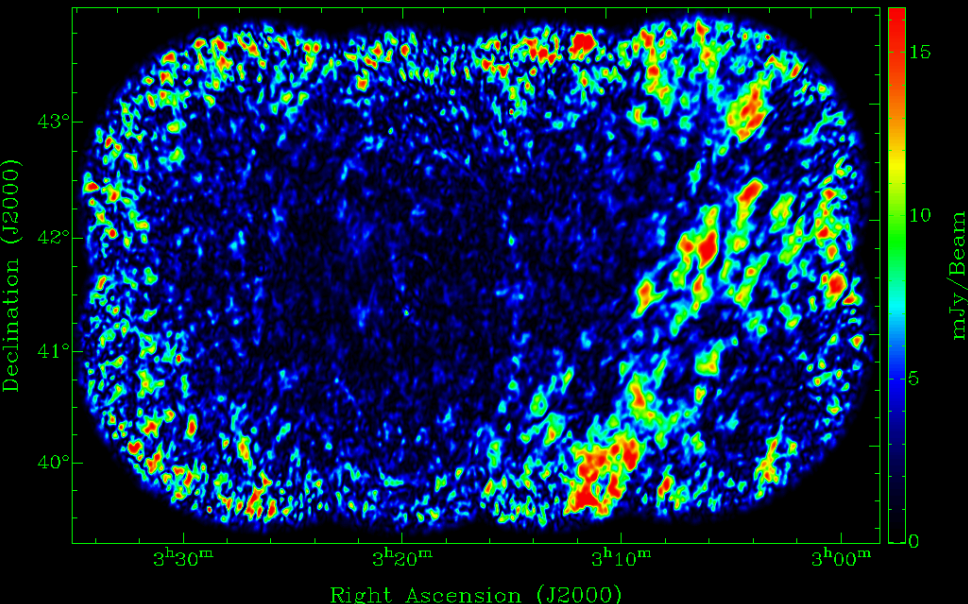
STOKES: 1.800000e+01



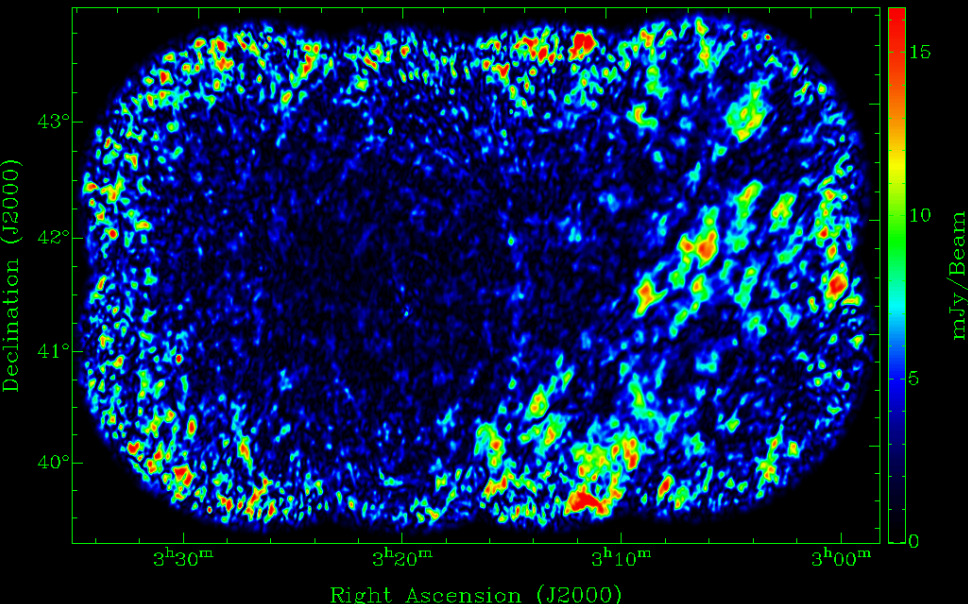
STOKES: 2.100000e+01



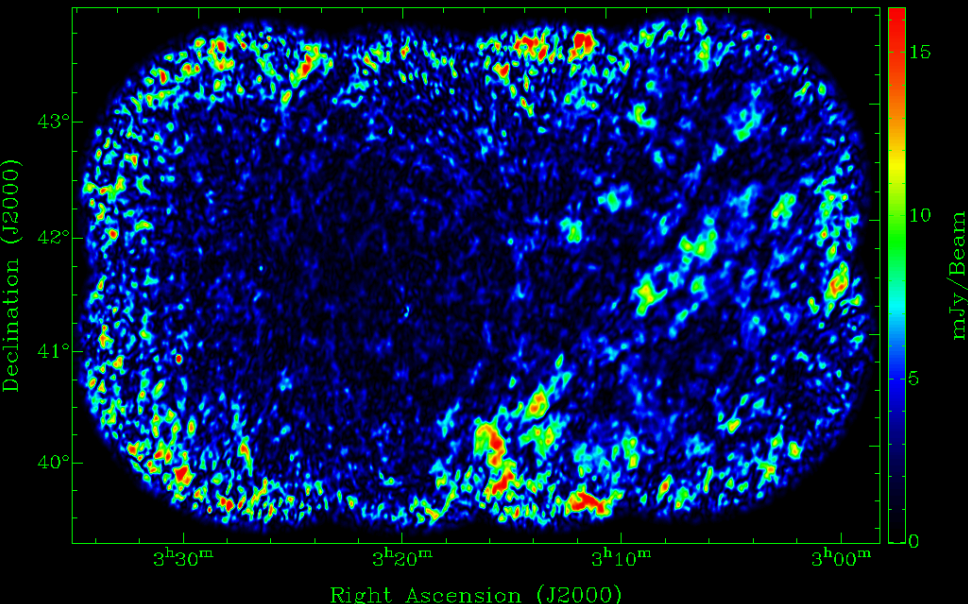
STOKES: 2.400000e+01



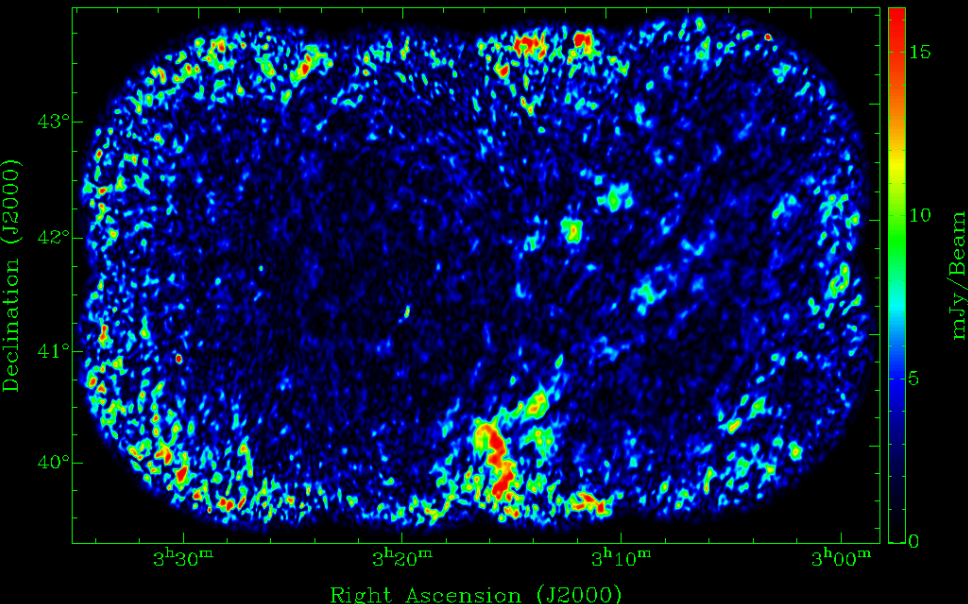
STOKES: 2.700000e+01



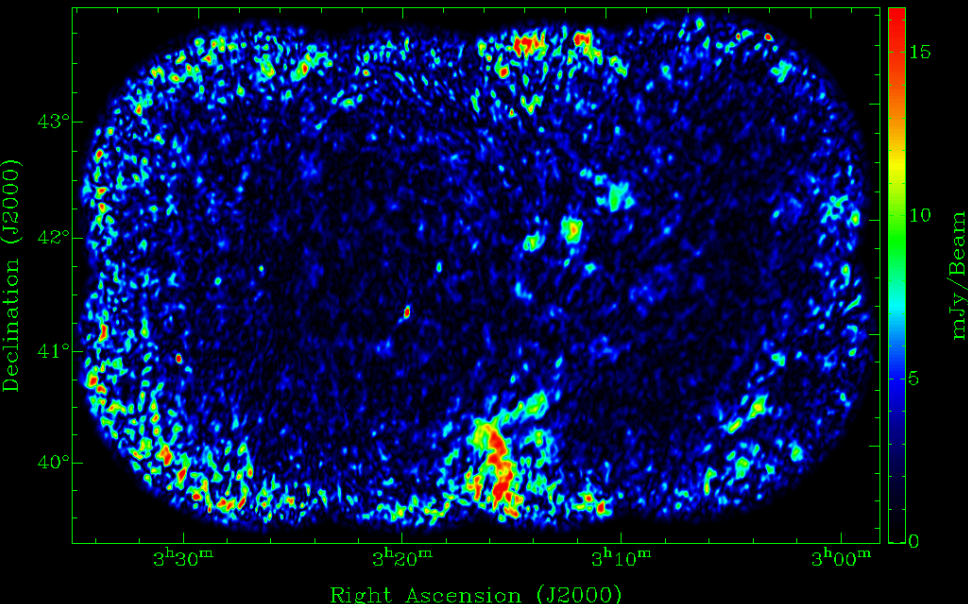
STOKES: 3.000000e+01



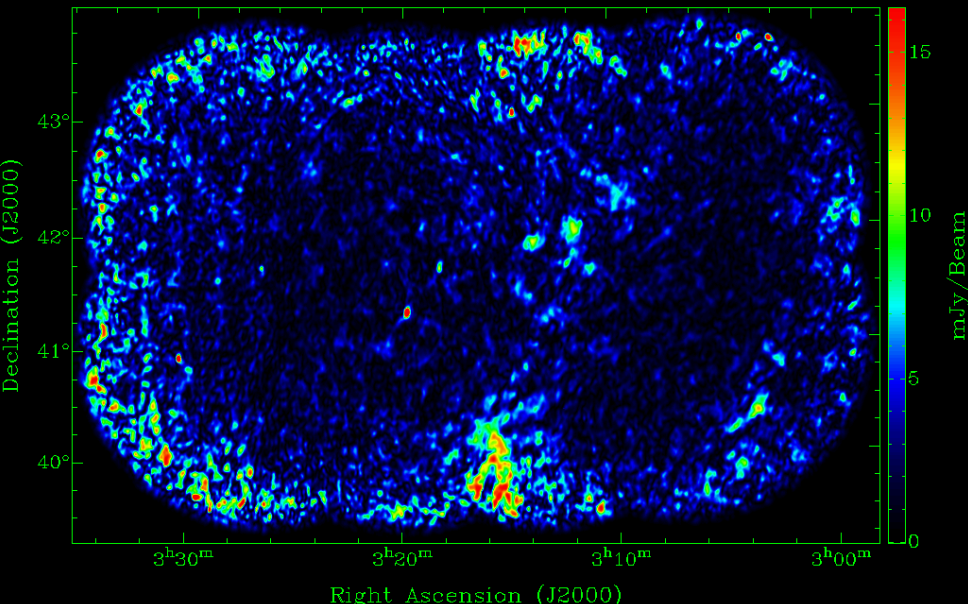
STOKES: 3.300000e+01



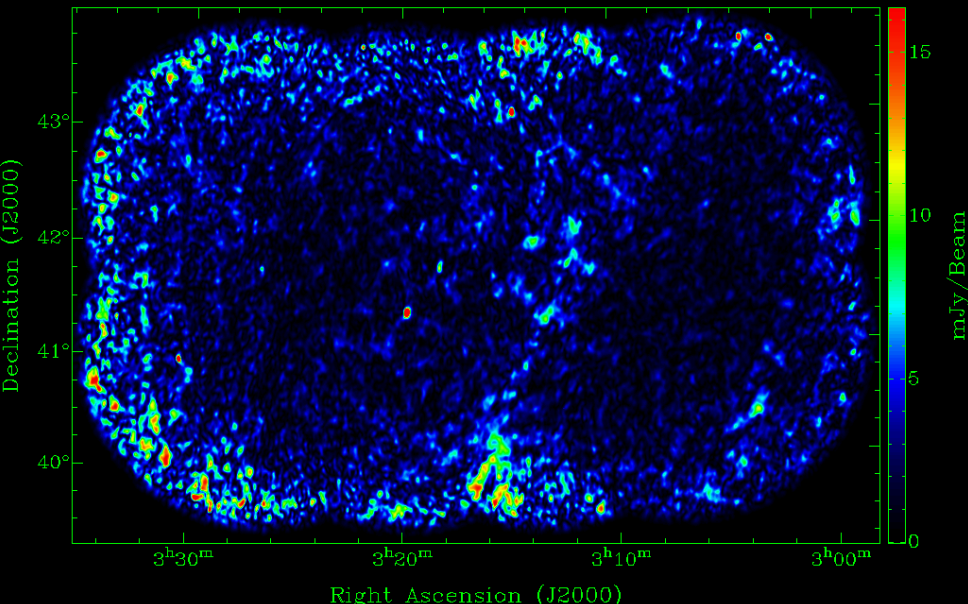
STOKES: 3.600000e+01



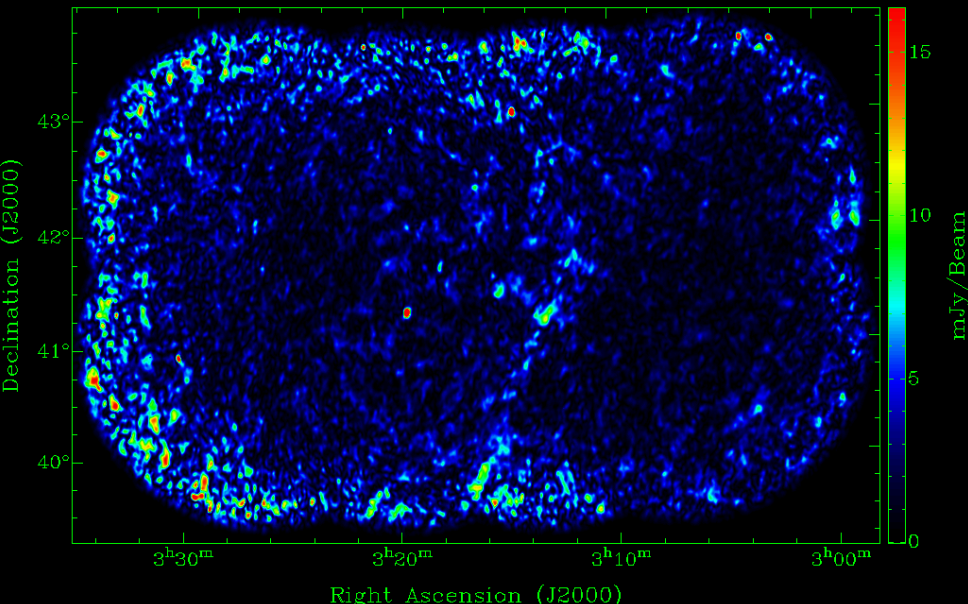
STOKES: 3.900000e+01



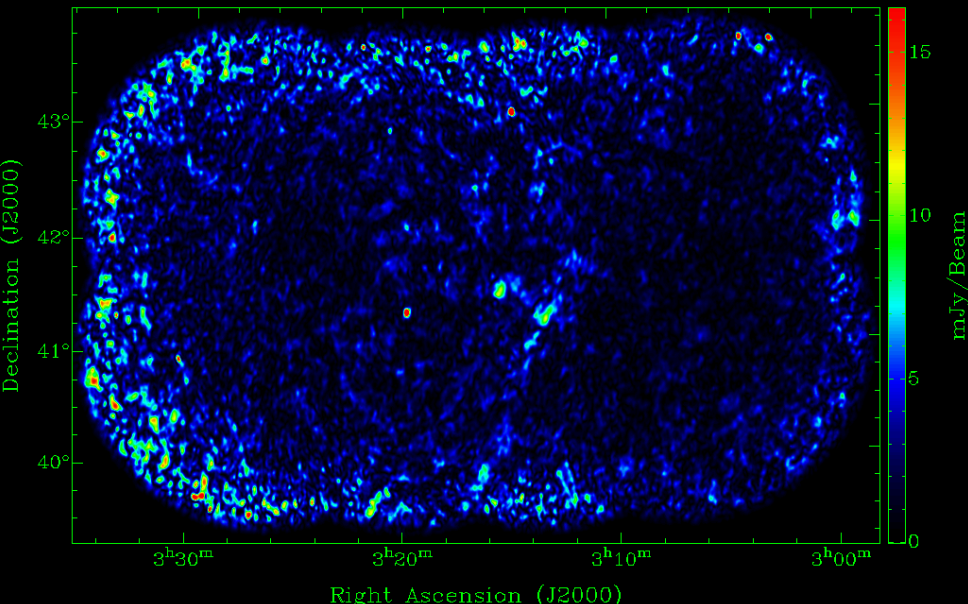
STOKES: 4.200000e+01



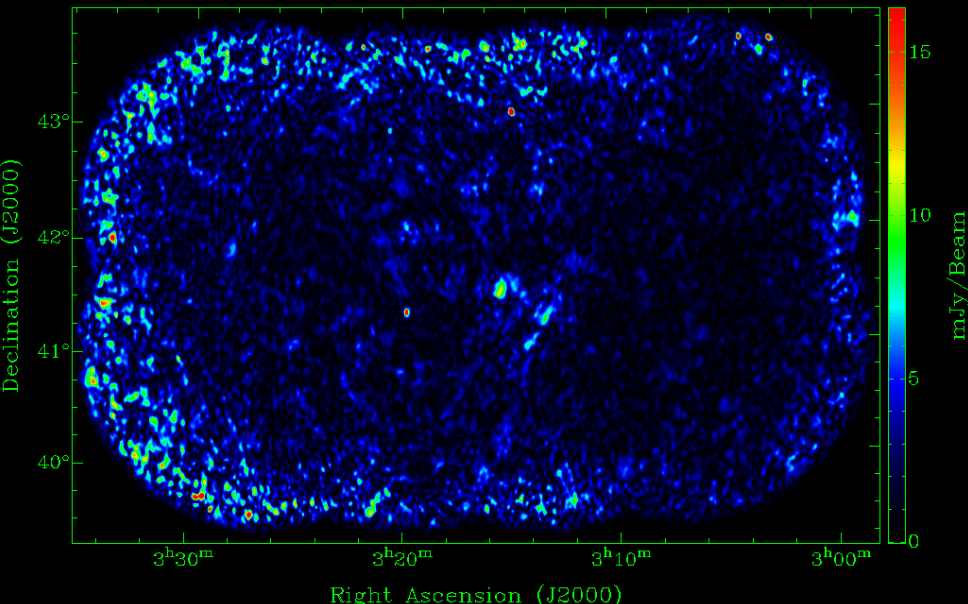
STOKES: 4.500000e+01



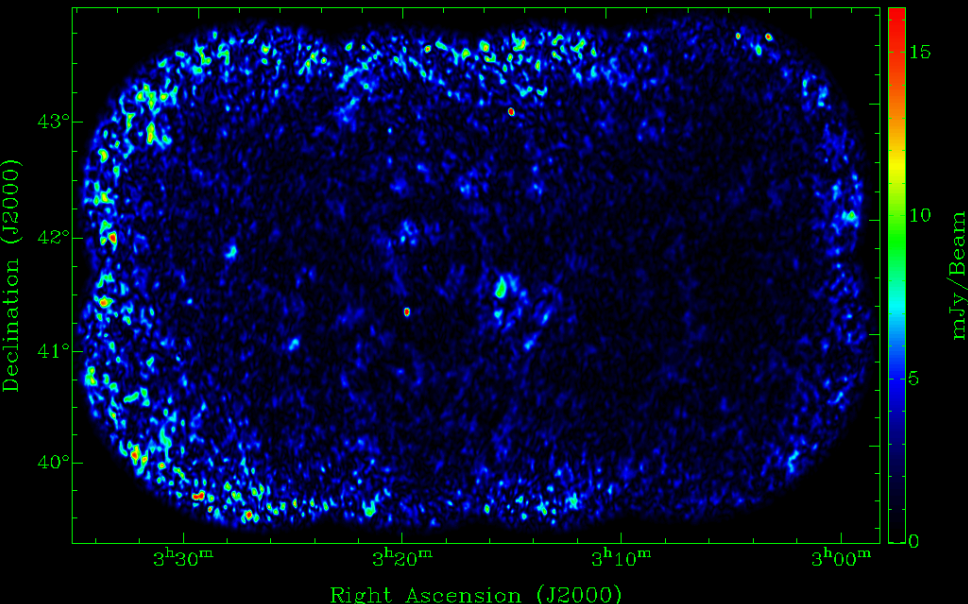
STOKES: 4.800000e+01



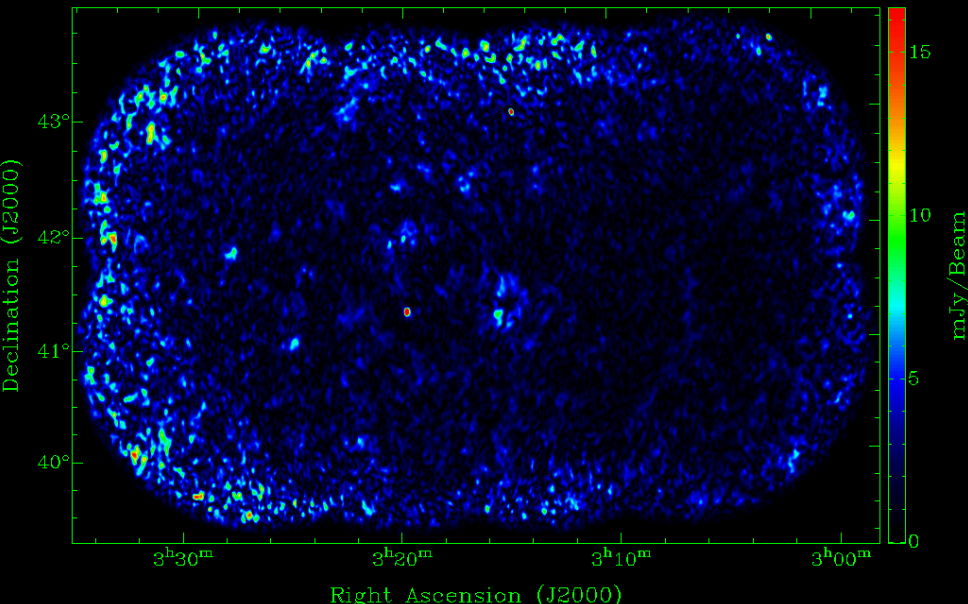
STOKES: 5.100000e+01



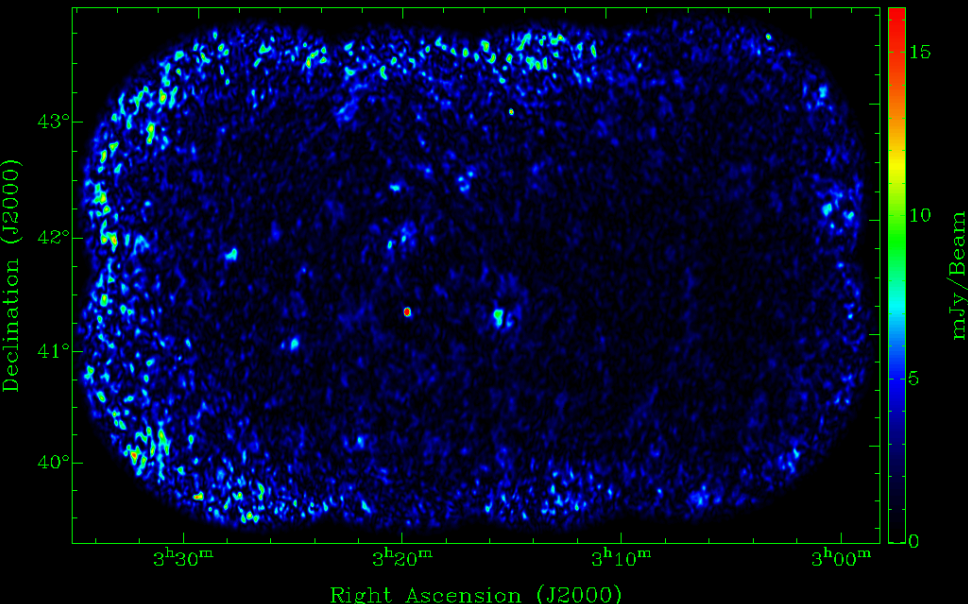
STOKES: 5.400000e+01



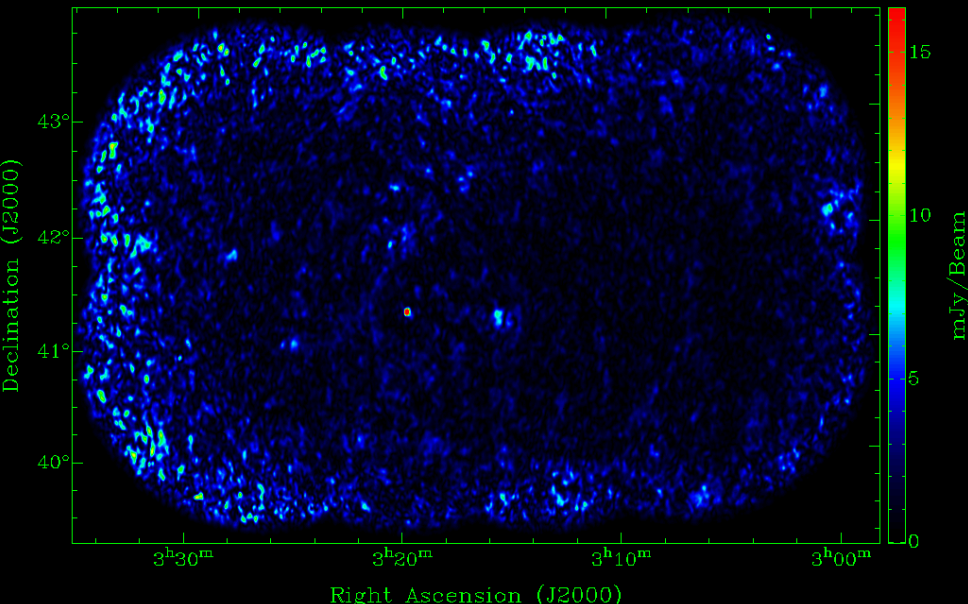
STOKES: 5.700000e+01



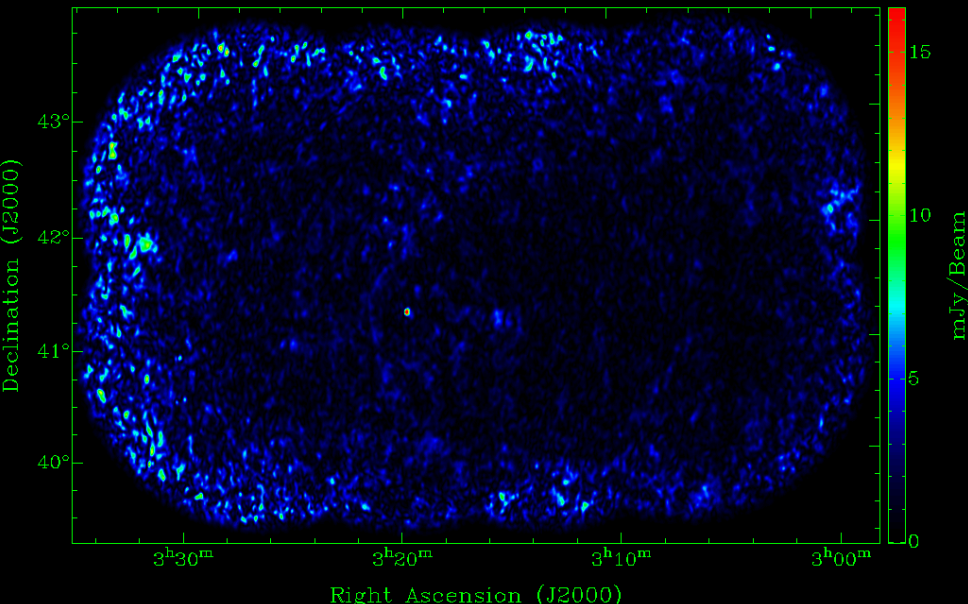
STOKES: 6.000000e+01



STOKES: 6.300000e+01



STOKES: 6.600000e+01



STOKES: 6.900000e+01

